# P22 Viral Capsids as Nanocomposite High-Relaxivity MRI Contrast Agents

Shefah Qazi,[†,‡,§] Lars O. Liepold,[†,‡,§] Md Joynal Abedin,[†,‡] Ben Johnson,[†,‡] Peter Prevelige,[∥] Joseph A. Frank,[⊥,#] and Trevor Douglas*[,†,‡]

[†]Chemistry and Biochemistry Department and [‡]Center for Bio-Inspired Nanomaterials, Montana State University, Bozeman, Montana, 59717, United States

[∥]Department of Microbiology, University of Alabama at Birmingham, Birmingham, Alabama 35294, United States

[⊥]Frank Laboratory, Radiology and Imaging Sciences, Clinical Center, and [#]National Institute of Biomedical Imaging and Bioengineering, National Institutes of Health, Bethesda, Maryland 20892, United States

**S** *Supporting Information*

**ABSTRACT:** Attachment of multiple chelated $Gd^{3+}$ ions to the interior of bacteriophage P22 viral capsids affords nanoscale MRI contrast agents with extremely high relaxivity values. Highly fenestrated "wiffleball" morphology is unique to P22 and assures water exchange between the environment and interior cavity of the capsid. The cavity of P22 "wiffleball" was functionalized with a branched oligomer comprising multiple DTPA−Gd complexes resulting in an impressive payload of 1,900 $Gd^{3+}$ ions inside each 64 nm capsid. High relaxivities of $r_{1,ionic} = 21.7$ mM$^{-1}$ s$^{-1}$ and $r_{1,particle} = 41,300$ mM$^{-1}$ s$^{-1}$ at 298



P22 'wiffleball' viral capsid
$r_1$ ionic = 21.7 mM$^{-1}$ s$^{-1}$
$r_1$ particle = 41,300 mM$^{-1}$ s$^{-1}$
298K, 28MHz
1,900 DTPA-Gd complexes per 64nm capsid

K, 0.65 T (28 MHz) are reported, with $r_1/r_2$ ratio of 0.80 and optimized rotational correlation time for this system. Specific design modifications are suggested for future improvements of viral capsid-based MRI contrast agents directed toward clinical translation.

**KEYWORDS:** *viral capsid, VLP, bacteriophage P22, magnetic resonance imaging, MRI, imaging agent, contrast agent, T1, relaxivity, gadolinium, DTPA−Gd, azide−alkyne click chemistry, nanoparticle, nanocomposite, protein cages, payload*
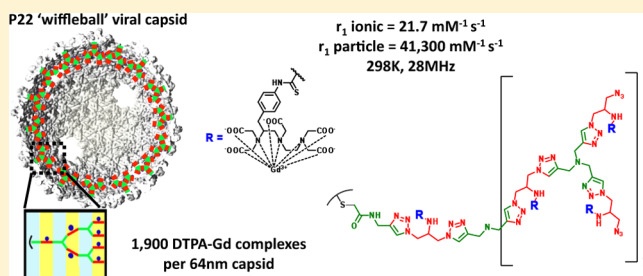
## INTRODUCTION

Magnetic resonance is often preferred over other imaging techniques because it employs harmless nonionizing radiation to produce high contrast images that distinguish between pathological and normal tissues. Low sensitivity of this technique can be overcome by the use of contrast agents which provide additional contrast between tissues. Inherent properties of small molecule contrast agents can be significantly improved by slowing the rate of molecular tumbling through conjugation to a macromolecular platform.[1,2] Various groups have explored dendrimers,[3] liposomes,[4,5] protein cages,[6,7] and more recently gold nanoparticles[8] as potential platforms for conjugation of small molecule contrast agents. Here, we explore noninfectious bacteriophage P22 viral capsids as nanoscale MRI contrast agents because of their inherent multivalency and slow tumbling rates resulting from their large size.[9−15] Viral capsids are advantageous over other macromolecular contrast agents because they have two distinct surfaces available for independent conjugation of multiple imaging and targeting agents to the same scaffold. These agents can potentially be administered at low doses and still produce very high-contrast images, meeting an important criterion for next-generation diagnostic tools.

Virus capsids are dynamic, self-assembling systems that form highly symmetrical, multivalent, monodisperse structures and can be produced in heterologous expression systems in large quantities as genome-free capsids. These capsids are exceptionally robust, remaining stable at a range of temperatures, pH, and buffers, and hence can be readily modified both genetically and chemically. Plant viruses and bacteriophages are particularly desirable in developing nanocomposites for applications in biomedicine because they are less likely to be pathogenic in humans.[16] Some virus-based systems that have been used for encapsulation of imaging agents include cowpea chlorotic mottle virus (CCMV),[13] cowpea mosaic virus (CPMV),[15] and bacteriophages Qβ[14] and MS2.[10−12] P22 bacteriophage, approximately double in size, allows for a much greater payload of imaging agent per capsid. It can undergo transformation to a "wiffleball" form, creating a fenestrated capsid structure which allows small molecules to freely diffuse between the external medium and the capsid interior.[17−19] The substantial size of the

interior cavity can be more efficiently utilized through incorporation of an oligomer network coupled to multiple small molecule imaging agents.

Here, we explore the genetically modified P22 capsid in its "wiffleball" architecture with site-specific thiol reactive residues at the 118 position as a $T_1$ Gd-based MRI contrast agent. Azide−alkyne click chemistry was used to synthesize a branched oligomeric network conjugated to DTPA−Gd complexes under optimal conditions,[15] and the influence of individual factors that affect the overall relaxivity behavior of the viral capsid nanocomposite was examined.[20] The P22 nanocomposite has a higher loading capacity of imaging agents than previously described systems and as a result provides an extremely high relaxivity per particle.

## EXPERIMENTAL SECTION

All materials were analytical grade and purchased from either Sigma-Aldrich or Fisher Scientific and used as received unless otherwise noted. All water was deionized using a NANOpure water purification system. Dynamic light scattering measurements were taken on a 90Plus particle size analyzer (Brookhaven). The synthesis of N-propargyl bromoacetamide and 2-azido-1-azidomethyl-ethylamine has been reported previously.[7] The p-SCN-Bn-DTPA was purchased from Macrocyclics.

**Mutagenesis.** The P22 (K118C) point mutation was made using established polymerase chain reaction protocols (Qiagen) using pET-3a based plasmids encoding genes for scaffolding and coat protein. The amplified DNA was transformed into CaCl$_2$ treated competent *Escherichia coli* strain BL21 (DE) and selected for ampicillin resistance.[21]

**Protein Purification.** Transformed BL21 (DE) *E. coli* was grown in 1 L cultures inoculated with 1 mL of starter culture (37 °C, 220 rpm). After 2 h (OD$_{600}$ = 0.6), the cultures were induced with 1 mM IPTG and grown for 4 more hours. Cells were harvested by centrifugation at 3700g for 20 min. The cells were resuspended in PBS pH 7.6 and were incubated with DNase, RNase, and lysozyme (all Sigma-Aldrich) for 30 min at room temperature. Cells were lysed further by sonication on ice (Branson Sonifier 250, Danbury, CT, power 4, duty cycle 50%, 3 × 5 min with 3 min intervals). Bacterial cell debris was removed via centrifugation at 12000g for 45 min. The supernatant was then loaded on a 35% sucrose cushion and centrifuged at 48,000 rpm for 50 min in an ultracentrifuge (50.2Ti ultra centrifuge rotor). The resulting virus pellet was resuspended in PBS pH 7.0 and dialyzed to remove sucrose. The P22 empty shells (ES) were prepared by repeated extraction of scaffolding protein with 0.5 M guanidine-HCl.[19] Purified ES were heated at 75 °C for 20 min to obtain P22 wiffleball (WB).[22] P22 WBs were further purified by 5−20% sucrose gradient centrifugation and dialyzed against buffer to remove residual sucrose. Each individual capsid form was routinely characterized using SDS−PAGE, native agarose gels, transmission electron microscopy (TEM, Leo 912 AB), and dynamic light scattering (DLS, Brookhaven 90Plus, Brookhaven, NY).[23] The protein concentration was determined by absorbance at 280 nm using the extinction coefficient (44,920 M$^{-1}$ cm$^{-1}$).

**Synthesis of p-SCN-Bn-DTPA−Gd.** 2-(4-Isothiocyanatobenzyl)-diethylenetriaminepentaacetic acid (p-SCN-Bn-DTPA) (250 mg, 0.385 mmol, 128 mM) was treated with gadolinium-(III) chloride (157 mg, 0.424 mmol, 141 mM, 1.1 equiv) in water. The mixture was stirred for 3 h at room temperature,

followed by removal of solvent by lyophilization under reduced pressure. The yield was quantitative, and the slightly yellowish product was characterized by LC−MS. The product was used without further purification.

LC−MS: A cluster of isotopic peaks centered at 696.23- (±1,2,3,4) was found for SCN-Bn-DTPA−Gd (C$_{25}$H$_{32}$N$_{11}$O$_{10}$SGd). Theoretical value for C$_{22}$H$_{25}$N$_4$O$_{10}$SGd is centered at 696.116.

**Synthesis of Diazidopropylamine Conjugated to p-SCN-Bn-DTPA−Gd (DAA−DTPA−Gd).** p-SCN-Bn-DTPA (322 mg, 0.462 mmol, 154 mM) was dissolved in water in a small round-bottom flask. The pH of the solution was raised slowly to 8.5 with dilute NaOH solution. While stirring, 2-azido-1-azidomethyl-ethylamine (131 mg, 0.924 mmol, 308 mM, 2.0 equiv) was added slowly in the reaction mixture. The mixture was stirred overnight at room temperature. Lyophilization of the mixture under reduced pressure yielded a slightly yellowish solid product. Excess 2-azido-1-azidomethyl-ethylamine was removed by washing the crude product several times with methylene chloride. The yield was quantitative, and the product was characterized by LC−MS. This product was used without further purification for bioconjugation with protein cage.

LC−MS: A cluster of isotopic peaks centered at 837.145 (±1,2,3,4,5) was found for DAA−DTPA−Gd (C$_{25}$H$_{32}$N$_{11}$O$_{10}$SGd). Theoretical value for C$_{25}$H$_{32}$N$_{11}$O$_{10}$SGd is centered at 837.138.

**Synthesis of P22-AACC-Gd.** Unless otherwise noted, all reaction steps were done in HEPES buffer, pH 7.6. Each reaction product was purified by dialysis with molecular porous membrane (MWCO 12−14K). Concentrations were determined by UV−vis spectrometry by OD$_{280}$. Oligomer was incorporated in a stepwise fashion to yield P22-AACC-Gd. Briefly, in pH 6.5 HEPES buffer, P22 (K118C) WB (83.3 mg, 1.79 μmol, 1.79 mM) was reacted with N-propargyl bromoacetamide (3.6 mg, 17.9 μ mol, 17.9 mM, 10 equiv) by stirring 1 h at room temperature, followed by incubation at 4 °C overnight. The P22-alkyne was characterized by LC−MS.

LC−MS: M + H 46693 (found), M + H 46692 (calcd).

The P22-alkyne (75 mg, 1.61 μmol, 215 mM) was reacted with DAA−DTPA−Gd (13.5 mg, 16.1 μmol, 2.15 M, 10 equiv) through Cu-catalyzed azide−alkyne coupling reaction.[24] Briefly, a 1:5 mixture of CuSO$_4$ and THPTA ligand[25] was prepared and added to the reaction mixture to achieve a final concentration of 0.90 mM Cu(I) and 4.5 mM THPTA ligand. This was followed by addition of sodium ascorbate and amino guanidine, both with final concentrations of 10.15 mM. The reaction vial was purged with N$_2$, sealed, and stirred for 1 h at room temperature and incubated overnight with stirring at 4 °C. The reaction mixture was treated with 12-fold excess of 0.5 M EDTA, pH 8.0 to chelate Cu ions associated with the P22 capsid derivatives. The resulting product was reacted with tripropargyl amine and DAA−DTPA−Gd in a stepwise fashion for a total of four more reactions under similar conditions as described above,[7] until a theoretical yield of seven DAA−DTPA−Gd were incorporated per subunit of P22 wiffleball. The intact P22-AACC-Gd overall recovery was 44.4% (37 mg, 0.80 mol, 8.0 mM).

**Multiangle Light Scattering.** P22 and P22-AACC-Gd were injected using an Agilent 1200 autosampler with PBS pH 7.3 and 200 ppm azide at 0.7 mL/min as the running buffer. The buffer was degassed using an inline degasser. Samples were run over a WTC-100S5G guard column (Wyatt Technology
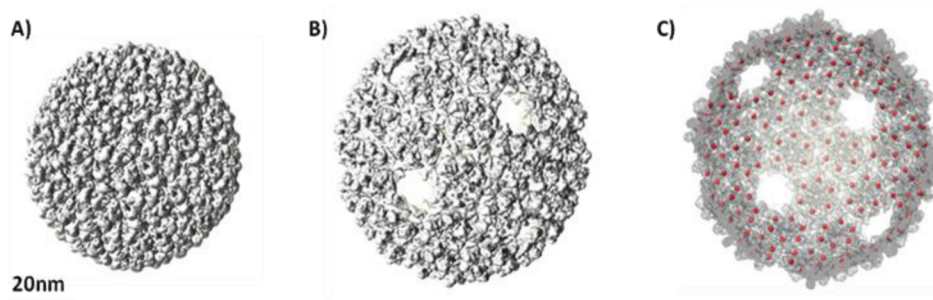
**Figure 1.** Cryo-EM reconstructions: (A) P22 PC procapsid (pdb 3IYI),[29] (B) P22 WB wiffleball (pdb 3IYH),[29] (C) P22 WB half cutaway view of capsid interior with residue 118 highlighted as red spheres.

Corporation) and a WTC-100S5 SEC column designed specifically for MALS (Wyatt Technology Corporation). The eluant was monitored using an in-line UV−vis detector on the Agilent system as well as a Dawn Heleos 8 MALS detector and an Optilab T-rex RI detector (Wyatt Technology Corporation). All data were analyzed using ASTRA software from Wyatt. Samples were stored in the autosampler at room temperature, and the sample chamber in the RI detector was held at 25 °C to reduce thermal drift. Molecular weights were determined from MALS and RI signals using the ASTRA software, and a d$n$/d$c$ value of 0.185 was used for all proteins.

**Transmission Electron Microscopy.** P22 and P22-AACC-Gd were imaged by transmission electron microscopy (Leo 912 AB) by negatively staining the sample with 2% uranyl acetate on Formvar carbon coated grids. Average diameters were determined from measurements of 10 particles for each sample.

**Denaturing Gel Assay.** P22 and P22-AACC-Gd were analyzed using SDS-PAGE on 10−20% gradient Tris-glycine gels (Lonza).

**Nuclear Magnetic Resonance Dispersion (NMRD).** $T_1$ and $T_2$ measurements were carried out on a variable field relaxometer. The longitudinal ($T_1$) and transverse ($T_2$) relaxation rate constants of P22-AACC-Gd were measured using an inversion−recovery and Carr−Purcell−Meiboom−Gill (CPMG) pulse sequence with 32 incremental tau values, respectively.[13] The measurements were collected for a range of Larmor frequencies between 2 and 62 MHz (0.05−1.5 T) at 298 K. Values for $r_1$, $r_2$, $q$, $\tau_M$, and $\tau_R$ were determined by fitting the raw data to a Solomon−Bloembergen−Morgan (SBM) analytical model for relaxivity as previously described.[6] All plots were produced using Mathcad 14.0.

**Gadolinium Concentration.** The gadolinium (Gd) concentration of P22-AACC-Gd was analyzed by NMR (300 MHz Bruker NMR) through adaptation of a published procedure.[12,26] A sample was prepared by digesting P22-AACC-Gd overnight in 30% $HNO_3$ at room temperature. A standard curve using $GdCl_3$ ranging from 0.3 $\mu$M to 1968.3 $\mu$M was used for quantification. The Gd concentration was further verified by inductively couple plasma mass spectrometry, ICP-MS, at Energy Laboratories (Billings, MT).

**Protein Concentration.** Modification to standard procedure for amino acid analysis was used.[27] Briefly, P22-AACC-Gd was spun down in a rotary evaporator until the sample was completely dry. A solution of 6 N HCl containing 1% phenol was added to the sample. The sample was digested under anaerobic conditions for 18 h at 110 °C, 20 psi. The acid from the digested sample was removed by a rotary evaporator. The sample was resuspended in $H_2O$ and 1% formic acid. Standards of amino acids were prepared in 6 N HCl ranging from 1.0 $\mu$M

to 2500 $\mu$M. ESI-Q-TOF mass spectrometry (Q-TOF Premier, Waters) interfaced to a Waters UPLC was used to determine presence of most abundant amino acids. A standard curve was made using best fit amino acid data. The peak intensities correlating to amino acids in P22-AACC-Gd were fit to the standard curve to extrapolate amino acid concentrations, which were used to calculate the protein concentration based on the amino acid sequence of P22.

## RESULTS AND DISCUSSION

In this work, we have utilized the P22 capsid as a synthetic template for the development of Gd-based $T_1$ MRI contrast agents because of its large interior cavity and our ability to take advantage of site specific modifications to the capsid. When bacteriophage P22, which naturally infects *Salmonella typhimurium*, is recombinantly expressed in *E. coli*, it self-assembles into a 58 nm procapsid structure from 420 identical subunits of coat protein and between 60 and 300 copies of an internal scaffold protein (Figure 1A).[18,19] The capsid can be induced to undergo a series of structurally characterized morphological transformations from the procapsid (PC) form.[17,28] Upon heating of P22 procapsid to 75 °C, the capsid expands to 64 nm causing the capsid wall to become thinner and selectively release all twelve of its icosahedral pentamers to produce the wiffleball morphology (WB), creating a hollow nanocontainer with 10 nm pores (Figure 1B) at the 5-fold axes.[22,29] The wiffleball form is used in this study due to its near double increase in volume as compared to the PC form, and because the highly robust and porous structure allows for free molecular access across the protein shell. A single-point mutation in the wild-type P22 coat protein, K118C, was utilized for site-specific modification with a branched oligomer using azide−alkyne click chemistry (AACC). The 118C mutation introduces an addressable thiol in each of the 420 subunits of the P22 capsid, and high-resolution structural models of the P22 capsid suggest that this site is mostly exposed to the internal surface (Figure 1C).[29]

Azide−alkyne click chemistry (AACC) is a well-established orthogonal oligomerization technique compatible with protein architectures. The reaction takes place between azide and alkyne moieties in the presence of a Cu(I) catalyst and an appropriate ligand to form a 1,4-substituted triazole. The internal oligomerization of P22 wiffleball was accomplished using previously described methods.[7,25] Reaction was initiated from the 118C mutation site after reaction of the thiol with *N*-propargyl bromoalkyne to create P22-alkyne (Figure 2A, Scheme 1). 2-Azido-1-azidomethyl-ethylamine (DAA) was coupled to 2-(4-isothiocyanatobenzyl)-diethylene-triamine pentaacetic acid gadolinium (*p*-SCN-Bn-DTPA−Gd) to create the
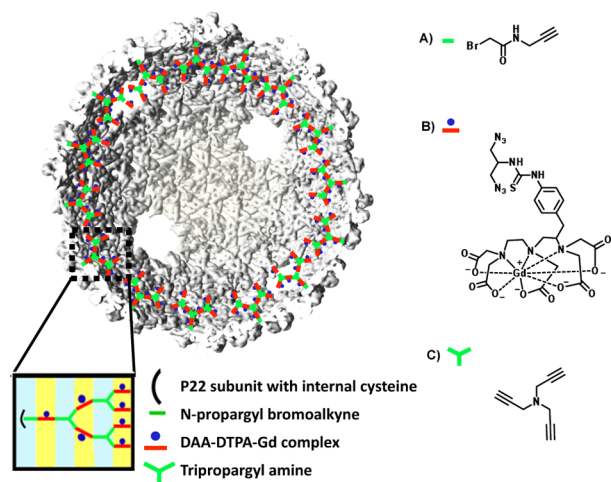
**Figure 2.** Theoretical incorporation of seven DAA−DTPA−Gd complexes per subunit of P22 WB. Monomers used for synthesis of branched oligomer (A) *N*-propargyl bromoalkyne, (B) 2-azido-1-azidomethyl-ethylamine coupled to 2-(4-isothiocyanatobenzyl)-diethylene-triamine pentaacetic acid gadolinium (DAA−DTPA−Gd complex), (C) tripropargyl amine.

bifunctional monomer (DAA−DTPA−Gd) (Figure 2B, Scheme 1) used in the oligomerization reaction. A branched oligomeric structure was synthesized by reaction of DAA−DTPA−Gd with the P22-alkyne, followed by reaction with tripropargyl amine (Figure 2C, Scheme 1) in a stepwise series of reactions to produce P22-AACC-Gd, until theoretical incorporation of seven DAA−DTPA−Gd moieties per subunit was achieved (Figure 2, Scheme 1).

Physical characterization of the resulting nanocomposite suggested no increase in overall particle size of P22-AACC-Gd compared to P22 WB with a relative increase in mass,

indicating that oligomer growth was confined to the interior of the capsid. P22-AACC-Gd was purified by size exclusion chromatography, and the elution time was identical to that of the P22 WB, indicating no change in the overall particle diameter (Figure 3C). Measurement of the particle sizes from transmission electron microscopy (Figure 3A) revealed mean diameters for P22 WB and P22-AACC-Gd of $57.4 \pm 2.5$ nm and $61.6 \pm 2.3$ nm, respectively. This was further confirmed by dynamic light scattering, which revealed a hydrodynamic diameter of $64.1 \pm 7.1$ nm for P22 WB and $63.1 \pm 5.9$ nm for P22-AACC-Gd (Figure 3B). Multiangle light scattering, coupled to HPLC size exclusion chromatography, also revealed that the size of the P22 capsid remained essentially unchanged for P22 WB and P22-AACC-Gd with an average radius of gyration of $29.7 \pm 0.06$ nm and $29.6 \pm 0.12$ nm, respectively (Figure 3C). Analysis of the MALS data additionally suggested an increase in mass for P22-AACC-Gd over the P22 WB, although absolute quantification is not possible because the refractive index increment ($dn/dc$) for the oligomer is not known. Further evidence of the mass increase associated with the oligomer growth was observed by sodium dodecyl sulfate−polyacrylamide gel electrophoresis (SDS−PAGE), which shows a shift in mobility of the subunit toward higher $M_w$ (Figure S1 in the Supporting Information) for P22-AACC-Gd, with no unmodified coat protein subunits visible. High $M_w$ species visible in the SDS−PAGE gel are consistent with some degree of intersubunit cross-linking between neighboring tripropargyl amine and DAA−DTPA−Gd "click" monomers. Together these data suggest that modification of the capsid is fairly uniform and is confined primarily to the interior of the P22 capsid.

Relaxivity measurements of P22-AACC-Gd were taken over a wide range of field strengths between 0.1 T and 1.4 T (Figure 4). For $r_{1,ionic}$ measurements, a peak centered at 0.6−0.8 T was

**Scheme 1. Overall Synthetic Scheme for Generating P22-AACC-Gd with Theoretical Incorporation of Seven DAA−Gd per Capsid**[a]
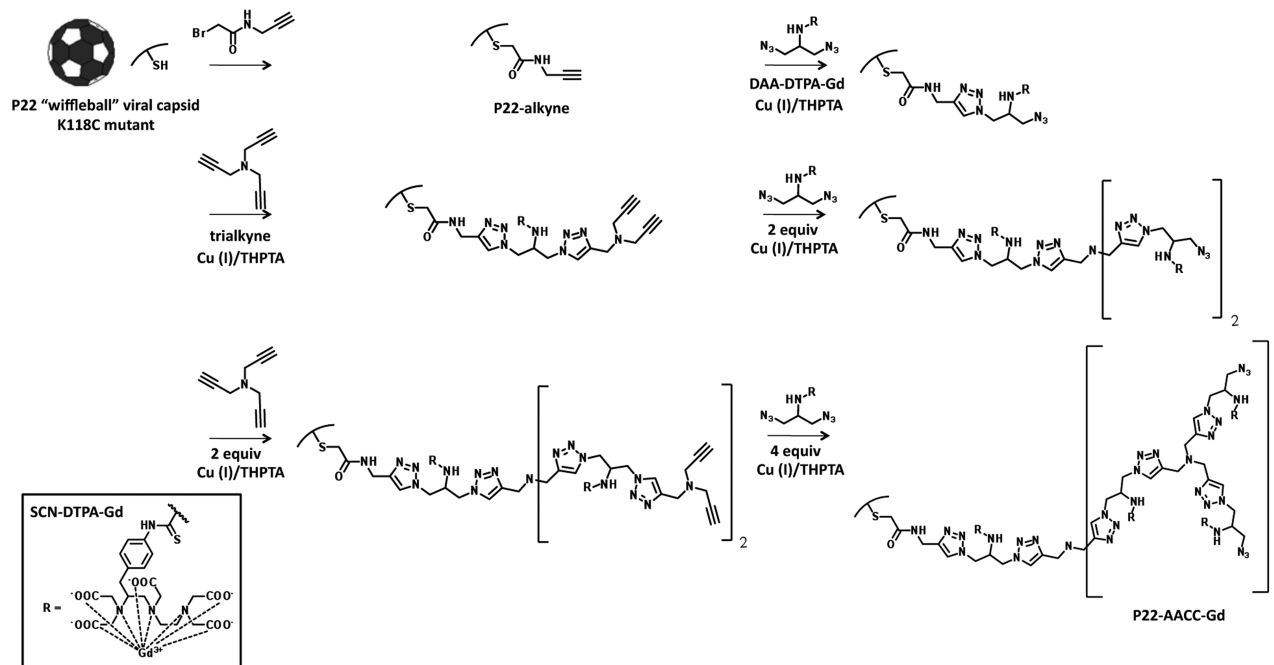


[a]Detailed experimental procedure can be found in previous reports.[7]
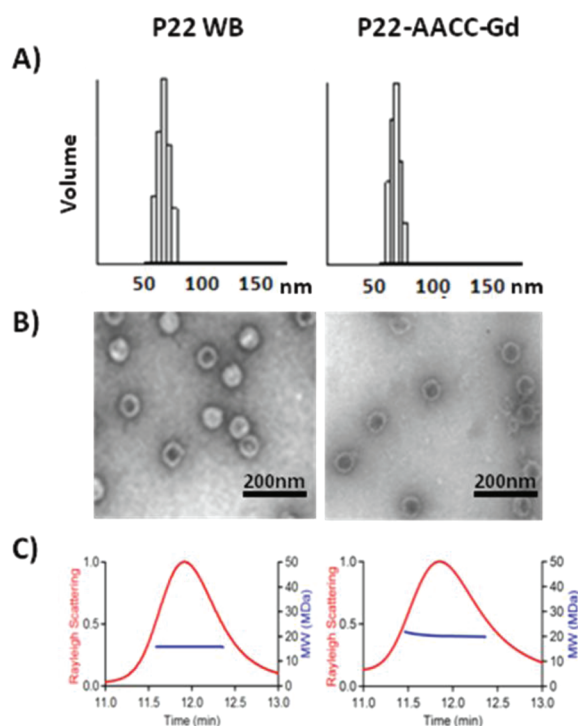
**Figure 3.** Similar capsid size before and after modification is reported using three different methods. (A) DLS (average diameter): P22 WB = 64.1 ± 7.1 nm, P22-AACC-Gd = 63.1 ± 5.9 nm. (B) TEM (average diameter): P22 WB = 57.4 ± 2.5 nm, P22-AACC-Gd = 61.6 ± 2.3 nm. (C) SEC-MALS (average radius): P22 WB = 29.7 ± 0.06 nm, P22-AACC-Gd = 29.8 ± 0.12 nm. An increase in molecular weight after modification (blue line) is indicative of oligomer growth within P22 cavity.
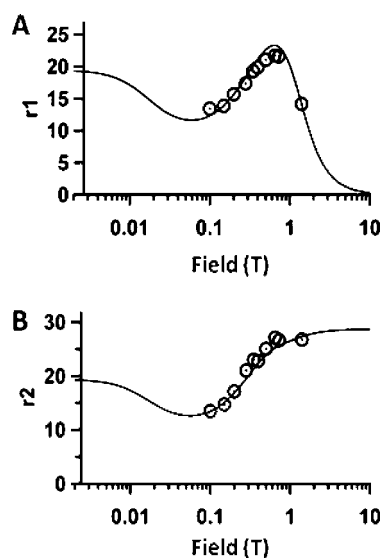


**Figure 4.** Nuclear magnetic dispersion profiles (NMRD) for P22-AACC-Gd, showing relaxivity as a function of field strength. The black circles indicate experimental data points which were fit to an SBM equation (eq S1 in the Supporting Information) where $r_1$ and $r_2$ were fit simultaneously (Table S1 in the Supporting Information). (A) $r_{1,ionic}$ NMRD profile. (B) $r_{2,ionic}$ NMRD profile.

observed (Figure 4a), which is characteristic of chelator–Gd complexes attached to macromolecular systems tumbling slowly in solution.[1,6,13,20,30] Maximum relaxivity occurred at

0.65 T, with an ionic relaxivity of $r_{1,ionic}$ = 21.7 mM$^{-1}$ s$^{-1}$, 6-fold greater than free DTPA–Gd,[31] and an exceedingly large per particle relaxivity, $r_{1,particle}$ = 41,300 mM$^{-1}$ s$^{-1}$ with considerable loading of 1,900 Gd per capsid. The $r_2$ profile (Figure 4b) is also consistent with previous findings for large macromolecular systems, with $r_{2,ionic}$ = 27.2 mM$^{-1}$ s$^{-1}$ and $r_{2,particle}$ = 51,800 mM$^{-1}$ s$^{-1}$. The absolute protein concentration of the modified P22 capsid was determined using standard amino acid analysis techniques, and relaxivity measurements were used to determine Gd concentration.

Nuclear magnetic resonance dispersion (NMRD) profiles for P22-AACC-Gd were attained from fitting relaxivity versus field strength to the Solomon–Bloembergen–Morgan (SBM) analytical model for relaxivity.[30,32−34] The fits were influenced by five parameters: the number of Gd-bound water molecules ($q$), the mean residence lifetime for Gd-bound water ($\tau_M$), the rotational correlation time ($\tau_R$), the magnitude of the zero field splitting interaction ($\Delta$), and the correlation time for transient zero field splitting fluctuation ($\tau_V$). A total of four fits were explored, with all fitting schemes resulting in similar values for $q$, $\tau_R$ and $\tau_M$. The best fit resulted in $q$ = 0.92, as expected for DTPA–Gd complexes ($q$ = 1).[1] A rotational correlation time of $\tau_R$ = 160 ns agrees well with reported values for bioconjugation of DTPA–Gd complexes to macromolecular systems, which lead to high ionic relaxivities due to slower tumbling of the nanocomposite as compared to free DTPA–Gd.[6,35] A value for mean residence lifetime for water of $\tau_M$ = 530 ns is similar to that of Gd–DTPA alone ($\tau_M$ = 240 ns),[6] which suggests, overall, that incorporating DTPA–Gd complexes within the P22 cavity does not restrict water access. However, observation of a slight increase in $\tau_M$ could be explained due to obstruction of water access in the presence of the bulky oligomer network surrounding the Gd$^{3+}$ ions.

MRI contrast agents with high ratios between the longitudinal and transverse relaxivities ($r_1/r_2$) ranging from 0.5 to 0.9 are defined as optimally performing Gd-based $T_1$ contrast agents.[5,36] For P22-AACC-Gd, the $r_1/r_2$ ratios range from 0.80 to 0.53 for magnetic fields 0.65−1.4 T, with the highest ratio of 0.82 at 0.73 T. This compelled us to explore the effects of mean residence lifetime ($\tau_M$) and rotational correlation time ($\tau_R$) on relaxivity at this field strength. We plotted relaxivity ($r_{1,ionic}$) versus field strength using three different values for $\tau_M$ and $\tau_R$ (Figure 5): the experimentally determined value (green), a value above the experimental (blue), and a value below the experimental (red). This allowed us to visualize how relaxivity at 0.73 T (maximum peak height) is affected by altering $\tau_M$ (Figure 5a) and $\tau_R$ (Figure 5b). It becomes apparent that, while $\tau_R$ has been optimized for this system, the $\tau_M$ can be further improved. The mean residence lifetime of water, $\tau_M$, could be altered by conjugating a different small molecule chelator–Gd complex[35] to the P22-oligomer composite.

In order for virus capsid-based MRI contrast agents to be clinically translatable, it is necessary to evaluate their relaxivity performance at higher field strengths. Using P22-AACC-Gd as a model system, its relaxivity ($r_1$ and $r_1/r_2$) performance was assessed at a range of field strengths for a range of $\tau_M$ values (Figure S2 in the Supporting Information) using contour plots. Particular attention was paid to relaxivity values at 3 T, another field strength commonly used clinically. We chose to evaluate the system at three different $\tau_R$ values for $\tau_M$ = 533 ns (the established $\tau_M$ for our system). For $\tau_R$ = 0.1 ns (Figure S2c in the Supporting Information), the $\tau_R$ value for free DTPA–Gd
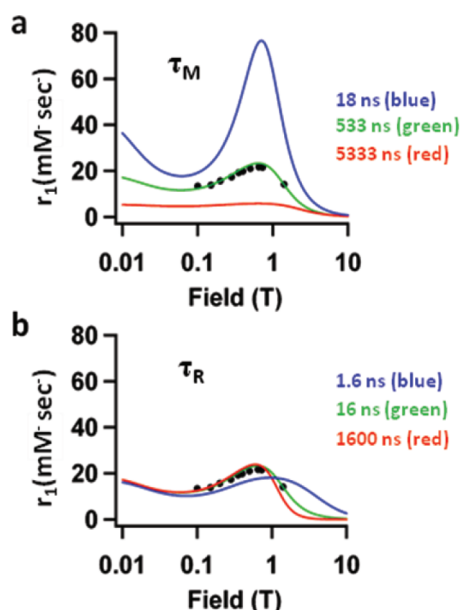
**Figure 5.** Plot of P22-AACC-Gd showing $r_1$ vs field strength for three different values of (a) $\tau_M$ [18 ns (blue), 533 ns (green), 5333 ns (red)] and (b) $\tau_R$ [1.6 ns (blue), 16 ns (green), 1600 ns (red)]. The black dots represent experimental values of $r_1$ for P22-AACC-Gd where the green line represents the best fit to the data. The plot illustrates that $\tau_R$ is optimized for P22-AACC-Gd at 0.73 T (maximum peak height), while $\tau_M$ could be further improved for this system.

complexes,[31] we see low $r_{1,ionic}$ of 3.2 mM$^{-1}$ s$^{-1}$ and high $r_1/r_2$ = 0.87. At a value of $\tau_R$ = 16 ns (Figure S2a in the Supporting Information), the established $\tau_R$ for our system, $r_{1,ionic}$ of 3.5 mM$^{-1}$ s$^{-1}$ is similar in value to free DTPA−Gd, while $r_1/r_2$ = 0.12 is lower than the optimal range. Reducing $\tau_R$ from 16 ns to 1 ns (Figure S2b in the Supporting Information) suggests an improvement in P22-AACC-Gd performance at 3 T, as $r_1$ is improved from 3.5 mM$^{-1}$ s$^{-1}$ to 13.0 mM$^{-1}$ s$^{-1}$ and the $r_1/r_2$ ratio from 0.12 to 0.78. Lower rotational correlation times ($\tau_R$) may be attained through conjugation of chelator−Gd complexes to a more flexible polymer. Utilizing an alternate polymer synthesis technique that creates a linear polymer instead of a branched polymer might result in greater degrees of freedom in terms of local motion of chelator−Gd complexes and will be explored in future work.

## CONCLUSIONS

In summary, we have synthesized a branched oligomer conjugated to multiple DTPA−Gd complexes inside of P22 "wiffleball" viral capsids. This resulted in one of the highest reported particle relaxivities for viral-capsid based systems and a significant improvement in ionic relaxivity over free DTPA−Gd. The rotational correlation time has been optimized for this system, while conjugation of different chelator−Gd complexes has been suggested for improvement of the mean residence lifetime. Better performance of this system at high field strengths has been suggested via conjugation of DTPA−Gd complexes to more flexible polymer networks inside the viral capsid, or alternatively DTPA−Gd may be attached to polymer via a more flexible linker.[8] Current efforts are focused on alternate polymerization techniques and addition of targeting ligands on the external surfaces of these viral nanoparticles.

## ASSOCIATED CONTENT

### Supporting Information
SDS−PAGE gel showing evidence of mass increase after modification, contour plot of relaxivity for P22-AACC-Gd, and additional details as discussed in the text. This material is available free of charge via the Internet at http://pubs.acs.org.

## AUTHOR INFORMATION

**Corresponding Author**
*Department of Chemistry and Biochemistry, Montana State University, Bozeman, MT 59717. Phone: (406) 994-6566. Fax: (406) 994-5117. E-mail: tdouglas@chemistry.montana.edu.

**Author Contributions**
§These authors contributed equally to this work

**Notes**
The authors declare no competing financial interest.

## REFERENCES

(1) Caravan, P. Strategies for increasing the sensitivity of gadolinium based MRI contrast agents. *Chem. Soc. Rev.* **2006**, *35* (6), 512−523.

(2) Cormode, D. P.; Jarzyna, P. A.; Mulder, W. J. M.; Fayad, Z. A. Modified natural nanoparticles as contrast agents for medical imaging. *Adv. Drug Delivery Rev.* **2010**, *62* (3), 329−338.

(3) Bumb, A.; Brechbiel, M.; Choyke, P. Macromolecular and dendrimer-based magnetic resonance contrast agents. *Acta Radiol.* **2010**, *51*, 751−767.

(4) Kamaly, N.; Miller, A. Paramagnetic Liposome Nanoparticles for Cellular and Tumour Imaging. *Int. J. Mol. Sci.* **2010**, *11*, 1759−1776.

(5) Mulder, W.; Strijkers, G.; van Tilborg, G.; Griffioen, A.; Nicolay, K. Lipid-based nanoparticles for contrast-enhanced MRI and molecular imaging. *NMR Biomed.* **2006**, *19* (1), 142−164.

(6) Liepold, L.; Abedin, M.; Buckhouse, E.; Frank, J.; Young, M.; Douglas, T. Supramolecular Protein Cage Composite MR Contrast Agents with Extremely Efficient Relaxivity Properties. *Nano Lett.* **2009**, *9* (12), 4520−4526.

(7) Abedin, M.; Liepold, L.; Suci, P.; Young, M.; Douglas, T. Synthesis of a Cross-Linked Branched Polymer Network in the Interior of a Protein Cage. *J. Am. Chem. Soc.* **2009**, *131* (12), 4346−4354.

(8) Ferreira, M. F.; Mousavi, B.; Ferreira, P. M.; Martins, C. I. O.; Helm, L.; Martins, J. A.; Geraldes, C. F. G. C. Gold nanoparticles functionalised with stable, fast water exchanging Gd3+ chelates as high relaxivity contrast agents for MRI. *Dalton Trans.* **2012**, *41* (18), 5472−5475.

(9) Allen, M.; Bulte, J.; Liepold, L.; Basu, G.; Zywicke, H.; Frank, J.; Young, M.; Douglas, T. Paramagnetic viral nanoparticles as potential high-relaxivity magnetic resonance contrast agents. *Magn. Reson. Med.* **2005**, *54* (4), 807−812.

(10) Anderson, E.; Isaacman, S.; Peabody, D.; Wang, E.; Canary, J.; Kirshenbaum, K. Viral nanoparticles donning a paramagnetic coat: Conjugation of MRI contrast agents to the MS2 capsid. *Nano Lett.* **2006**, *6* (6), 1160−1164.

(11) Datta, A.; Hooker, J.; Botta, M.; Francis, M.; Aime, S.; Raymond, K. High relaxivity gadolinium hydroxypyridonate-viral capsid conjugates: Nanosized MRI contrast agents. *J. Am. Chem. Soc.* **2008**, *130* (8), 2546−2552.

(12) Hooker, J.; Datta, A.; Botta, M.; Raymond, K.; Francis, M. Magnetic resonance contrast agents from viral capsid shells: A comparison of exterior and interior cargo strategies. *Nano Lett.* **2007**, *7* (8), 2207−2210.

(13) Liepold, L.; Anderson, S.; Willits, D.; Oltrogge, L.; Frank, J.; Douglas, T.; Young, M. Viral capsids as MRI contrast agents. *Magn. Reson. Med.* **2007**, *58* (5), 871−879.

(14) Pokorski, J.; Breitenkamp, K.; Liepold, L.; Qazi, S.; Finn, M. G. Functional Virus-Based Polymer−Protein Nanoparticles by Atom Transfer Radical Polymerization. *J. Am. Chem. Soc.* **2011**, *133* (24), 9242−9245.

(15) Prasuhn, D.; Yeh, R.; Obenaus, A.; Manchester, M.; Finn, M. G. Viral, M. R. I. contrast agents: coordination of Gd by native virions and attachment of Gd complexes by azide-alkyne cycloaddition. *Chem. Commun.* **2007**, *12*, 1269−1271.

(16) Steinmetz, N. F. Viral nanoparticles as platforms for next-generation therapeutics and imaging devices. *Nanomedicine* **2010**, *6* (5), 634−641.

(17) Earnshaw, W.; Casjens, S.; Harrison, S. Assembly of head of bacterophage P22 - X-ray difrraction from heads, proheads and related structures. *J. Mol. Biol.* **1976**, *104* (2), 387−410.

(18) King, J.; Lenk, E.; Botstein, D. Mechanism of head assembly and DNA encapsulation in Salmonella phage P22. II. Morphogenetic pathway. *J. Mol. Biol.* **1973**, *80* (4), 697−731.

(19) Prevelige, P.; Thomas, D.; King, J. Scaffolding protein regulates the polymerization of P22 coat subunits into icosahedral shells in vitro. *J. Mol. Biol.* **1988**, *202* (4), 743−757.

(20) Aime, S.; Cabella, C.; Colombatto, S.; Crich, S.; Gianolio, E.; Maggioni, F. Insights into the use of paramagnetic Gd (III) complexes in MR-molecular imaging investigations. *J. Magn. Reson. Imaging* **2002**, *16* (4), 394−406.

(21) Kang, S.; Uchida, M.; O'Neil, A.; Li, R.; Prevelige, P.; Douglas, T. Implementation of P22 Viral Capsids as Nanoplatforms. *Biomacromolecules* **2010**, *11* (10), 2804−2809.

(22) Teschke, C.; McGough, A.; Thuman-Commike, P. Penton release from P22 heat-expanded capsids suggests importance of stabilizing penton-hexon interactions during capsid maturation. *Biophys. J.* **2003**, *84* (4), 2585−2592.

(23) Kang, S.; Hawkridge, A.; Johnson, K.; Muddiman, D.; Prevelige, P. Identification of Subunit-Subunit Interactions in Bacteriophage P22 Procapsids by Chemical Cross-linking and Mass Spectrometry. *J. Proteome Res.* **2006**, *5* (2), 370−377.

(24) Gupta, S.; Kuzelka, J.; Singh, P.; Lewis, W.; Manchester, M.; Finn, M. G. Accelerated Bioorthogonal Conjugation: A Practical Method for the Ligation of Diverse Functional Molecules to a Polyvalent Virus Scaffold. *Bioconjugate Chem.* **2005**, *16* (6), 1572−1579.

(25) Hong, V.; Presolski, S.; Ma, C.; Finn, M. G. Analysis and optimization of copper-catalyzed azide-alkyne cycloaddition for bioconjugation. *Angew. Chem., Int. Ed.* **2009**, *48* (52), 9879−9883.

(26) Crich, S.; Biancone, L.; Cantaluppi, V.; Esposito, D.; Russo, S.; Camussi, G.; Aime, S. Improved route for the visualization of stem cells labeled with a Gd-/Eu-chelate as dual (MRI and fluorescence) agent. *Magn. Reson. Med.* **2004**, *51* (5), 938−944.

(27) Bidlingmeyer, B. A.; Cohen, S. A.; Tarvin, T. L. Rapid analysis of amino acids using pre-column derivatization. *J. Chromatogr., B: Biomed. Sci. Appl.* **1984**, *336* (1), 93−104.

(28) Jiang, W.; Li, Z.; Zhang, Z.; Baker, M.; Prevelige, P.; Chiu, W. Coat protein fold and maturation transition of bacteriophage P22 seen at subnanometer resolutions. *Nat. Struct. Biol.* **2003**, *10* (2), 131−135.

(29) Parent, K.; Khayat, R.; Tu, L.; Suhanovsky, M.; Cortines, J.; Teschke, C.; Johnson, J.; Baker, T. P22 Coat Protein Structures Reveal a Novel Mechanism for Capsid Maturation: Stability without Auxiliary Proteins or Chemical Crosslinks. *Structure* **2010**, *18* (3), 390−401.

(30) Lauffer, R. Paramagnetic Metal-Complexes as Water Proton Relaxation Agents for Nmr Imaging - Theory and Design. *Chem. Rev.* **1987**, *87* (5), 901−927.

(31) Powell, H.; Dhubhghaill, O.; Pubanz, D.; Helm, L.; Lebedev, Y.; Schlaepfer, W.; Merbach, A. Structural and Dynamic Parameters Obtained from $^{17}$O NMR, EPR, and NMRD Studies of Monomeric and Dimeric Gd$^{3+}$ Complexes of Interest in Magnetic Resonance Imaging: An Integrated and Theoretically Self-Consistent Approach. *J. Am. Chem. Soc.* **1996**, *118* (39), 9333−9346.

(32) Helm, L. Relaxivity in paramagnetic systems: Theory and mechanisms. *Prog. Nucl. Magn. Reson. Spectrosc.* **2006**, *49* (1), 45−64.

(33) Helm, L.; Merbach, A. Inorganic and bioinorganic solvent exchange mechanisms. *Chem. Rev.* **2005**, *105* (6), 1923−1959.

(34) Helm, L.; Nicolle, G. L. M.; Merbach, R. E. Water and Proton Exchange Processes on Metal Ions. *Adv. Inorg. Chem.* **2005**, *57*, 327−379.

(35) Garimella, P. D.; Datta, A.; Romanini, D. W.; Raymond, K. N.; Francis, M. B. Multivalent, High-Relaxivity MRI Contrast Agents Using Rigid Cysteine-Reactive Gadolinium Complexes. *J. Am. Chem. Soc.* **2011**, *133* (37), 14704−14709.

(36) Na, H. B.; Song, I. C.; Hyeon, T. Inorganic Nanoparticles for MRI Contrast Agents. *Adv. Mater.* **2009**, *21* (21), 2133−2148.